

Molecular Imaging of Retinoic Acids in Live Cells Using Single-Chain Bioluminescence Probes

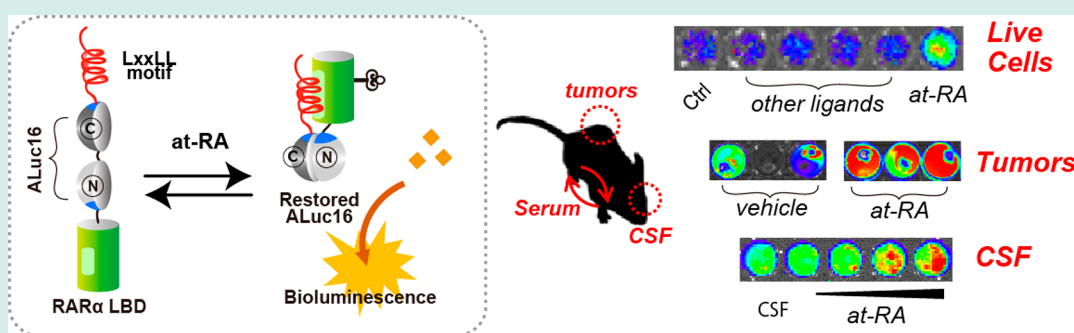
Sung Bae Kim,^{*,†,§} Rika Fujii,[†] Ryo Nishihara,[‡] Rajendran JC Bose,[§] Daniel Citterio,[‡] Koji Suzuki,[‡] Tarik F Massoud,[§] and Ramasamy Paulmurugan^{*,§}

[†]Research Institute for Environmental Management Technology, National Institute of Advanced Industrial Science and Technology (AIST), 16-1 Onogawa, Tsukuba 305-8569, Japan

[‡]Department of Applied Chemistry, Faculty of Science and Technology, Graduate School of Science and Technology, Keio University, 3-14-1 Hiyoshi, Kohoku-ku, Yokohama, Kanagawa 223-8522, Japan

[§]Molecular Imaging Program at Stanford, Bio-X Program, Stanford University School of Medicine, Stanford, California 94304, United States

Supporting Information



ABSTRACT: Retinoic acid (RA) is a key metabolite necessary for embryonic development and differentiation in vertebrates. We demonstrate the utility of genetically encoded, ligand-activatable single-chain bioluminescence probes for detecting RAs from different biological sources. We examined 13 different molecular designs to identify an efficient single-chain probe that can quantify RA with significant sensitivity. The optimal probe consisted of four components: the N- and C-terminal fragments of artificial luciferase variant-16 (ALuc16), the ligand binding domain of retinoic acid receptor α (RAR α LBD), and an LXXLL interaction motif. This probe showed a 5.2-fold greater bioluminescence intensity in response to RA when compared to the vehicle control in live mammalian cells. The probe was highly selective to all-trans-RA (at-RA), and highly sensitive in determining at-RA levels in cells derived from tumor xenografts created using MDA-MB-231 cells engineered to stably express the probe. We also detected RA levels in serum and cerebrospinal fluid. Using this probe, the detection limit for at-RA was $\sim 10^{-9.5}$ M, with a linear range of two orders. We present a highly useful technique to quantitatively image endogenous at-RA levels in live mammalian cells expressing novel single-chain bioluminescence probes.

KEYWORDS: retinoic acids, retinoic acid receptor, bioluminescence, protein–protein interactions, artificial luciferase, single-chain probe

INTRODUCTION

Retinoic acid (RA) is a biologically active form of vitamin A. All-trans-RA (at-RA) has effects on growth and cell differentiation, nervous system development, pattern formation, and tumorigenesis^{1,2} by regulating transcription of hundreds of genes through binding to retinoic acid receptors (RAR) α , β , γ , and peroxisome proliferator-activated receptor (PPAR) β/δ .³ The potential impact of RAs on human health has been well investigated with respect to its acute and chronic toxicity,^{4,5} especially to women and young children, including its teratogenicity.^{6–8} It is also known that at-RA is an effective chemotherapy agent for treating acute promyelocytic leukemia, and in inhibiting the in vivo development of carcinomas of breast, bladder, liver, lung, pancreas, prostate, ovaries, and

skin.^{9–11} Therefore, it is important to investigate the hormonal impacts of RA and its analogues in live mammalian cell models.

The binding of at-RA to the ligand-binding domain of RAR α (RAR α LBD) triggers an intramolecular conformational change and its dimerization, which recruits and binds to many coactivators via the common LXXLL motif. The activated RAR dimers translocate into the nucleus, where they bind to a specific sequence in the RA response elements (RAREs) of target genes, and finally activate transcription of

Received: February 25, 2019

Revised: April 12, 2019

Published: April 29, 2019

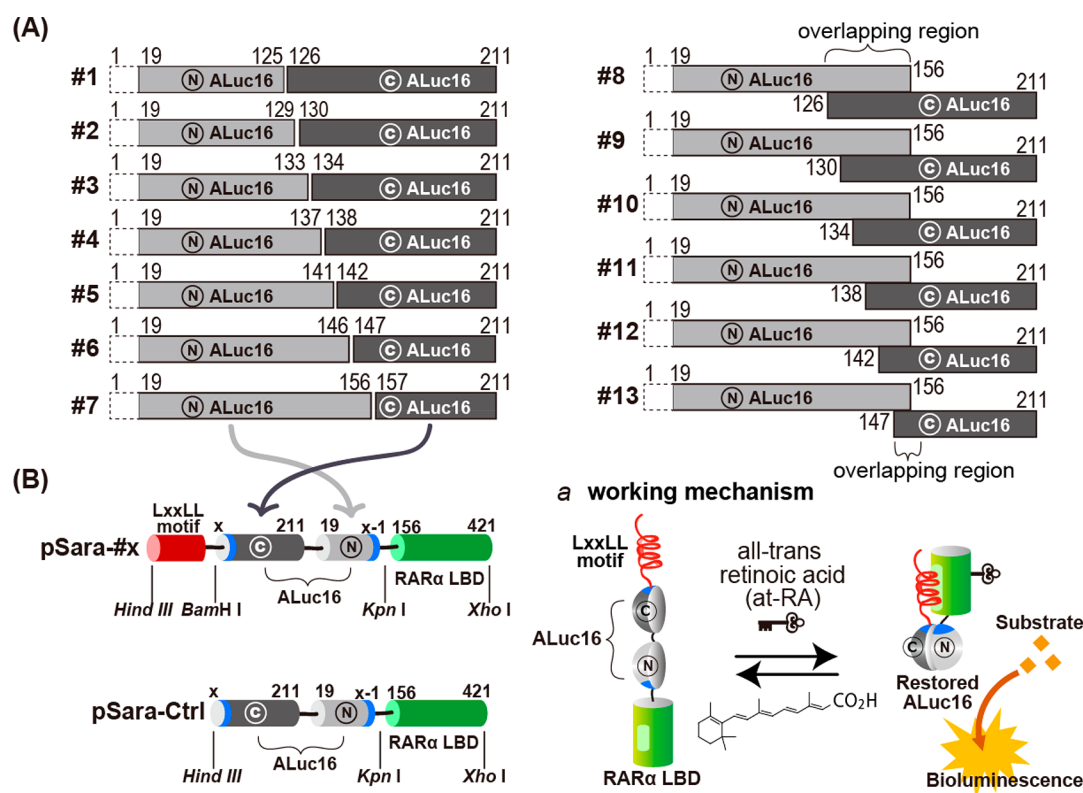


Figure 1. (A) Schematic diagrams of designed RAR probes for illuminating the activities of retinoic acids (RAs). The N- and C-terminal fragments are shown in light and dark gray colors. The secretion peptide (SP; 1–18 AA) at the N-terminal end was eliminated and marked by a dotted zone. (B) The cDNA constructs and the working mechanism of the single-chain probes. The blue zone symbolizes the active sites: ©ALuc16, the N-terminal fragment of artificial luciferase 16; ©ALuc16, the C-terminal fragment of artificial luciferase 16; RAR α LBD, the ligand binding domain of retinoic acid receptor α ; LXXLL motif, a common leucine-rich α -helical peptide of SRC1 coactivator protein.

many genes.¹ This RA-driven RAR activation process has previously been shown in transgenic mice.¹²

To date, two principle methods have been used to determine RA levels in living subjects: (1) monitoring using fluorescence resonance energy transfer (FRET) assays¹³ and (2) reporter gene assays using RAREs as promoters.¹⁴ In the FRET assay, the energy donor fluorescent protein (FP) and acceptor FP are fused to the N- and C-terminals of RAR α LBD. A RA-activated conformational change in RAR α LBD closely approximates the two FPs, which increases the FRET efficiency by altering the relative distance between the two proteins. However, this strategy suffers from autofluorescence. Further, the reporter gene assays usually require long stimulation times, until accumulation of sufficient amounts of reporter proteins in cells, typically 4 to 24 h.^{15,16} Thus, these techniques are not appropriate for depicting real-time dynamics of molecular events pertaining to RA.

We previously developed the concept of single-chain bioluminescence (BL) probes to quantitatively image hormonal activities of steroids, such as androgen, estrogen, and cortisol.^{17–21} However, it was unclear whether the basic strategy adopted would be practically useful in measuring an exogenous category of bioactive small molecules, including vitamins. Further, most of the previous studies have used lysates of cells transiently transfected with the reporter, and thus it was unclear if the same strategy would be transferable to mammalian cells and animal models developed from cells stably expressing a single-chain probe.

Here, we design a ligand-activatable single-chain BL probe by linking four essential components for imaging at-RA

activities. Thus, we fused four tandem motifs into a single chain: RAR α LBD, LXXLL motif, and the N- and C-terminal fragments of artificial luciferase 16 (ALuc16, GenBank MF817967). The probe was named “Sara”, from the abbreviation of single-chain BL assay probes for retinoic acids. Upon binding of at-RA to RAR α LBD in Sara, activation occurs on the LBD to interact with the adjacent LXXLL motif. This intramolecular protein–protein interaction (PPI) triggers approximation of the N- and C-terminal domains of ALuc16 (protein-fragment complementation), which reconstitutes its enzymatic activity in a RA-dependent manner.

We studied 13 different molecular designs to identify an optimal single-chain BL probe that can sensitively measure RA in different physiological body fluids. Among these various probes, Sara #12 showed selective activation in response to at-RA and was chosen for use in further studies in live mammalian cells and mouse models. We here show that BL is achieved through intramolecular complementation between the N- and C-terminal fragments of split-ALuc16, which is triggered by a PPI between the LXXLL motif and the RAR α LBD. We present these unique, efficient single-chain BL probes that illuminate the hormonal activities of RAs in body fluids and tumor xenografts using live mammalian cells stably expressing the sensors by ex vivo assay.

RESULTS AND DISCUSSION

Design of Single-Chain Probes for Measuring Retinoic Acids. We initially designed seven types of single-chain probes for measuring the activities of at-RAs (Sara #1–

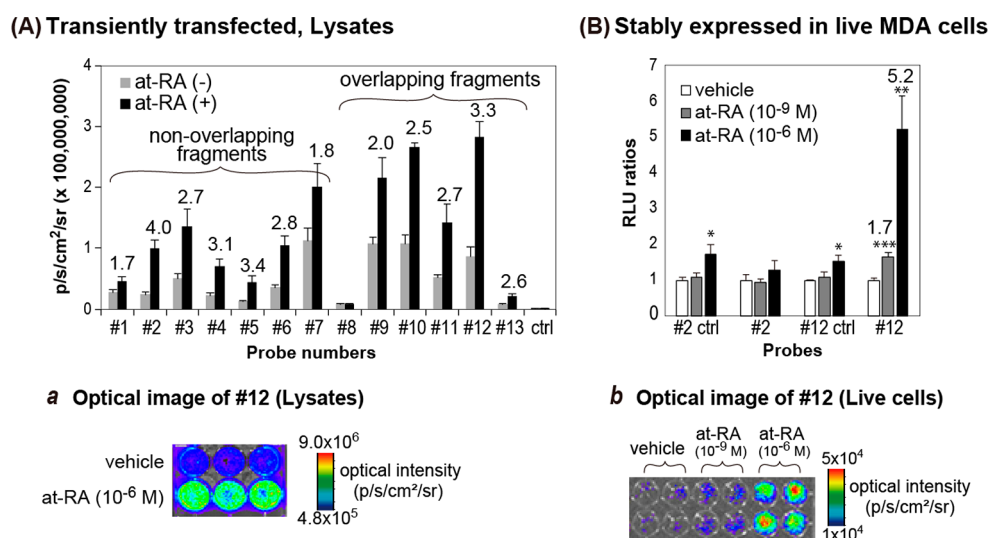


Figure 2. (A) Retinoic acid (RA)-activated optical intensities of the probes. The probes were transiently expressed in MDA-MB-231 cells. The optical intensities before and after addition of at-RA were determined. Inset a shows the optical image of the Sara #12. The values were independently measured in quadruplicates from a single experiment ($n = 4$). The p -values (student t test) are $*** \leq 0.001$ and $** \leq 0.01$. (B) The relative optical intensities of the Sara #2 ctrl, Sara #2, Sara #12 ctrl, Sara #12 in response to at-RA. Inset b shows the optical image of the probes. The values were independently measured in quadruplicates from a single experiment ($n = 4$). The p -values (student t test) are $*** \leq 0.001$ and $** \leq 0.01$.

Sara #7, Figure 1A). The single-chain probe consisted of the N- and C-terminal fragments of split-artificial luciferase 16 (ALuc16), a consensus α -helical binding sequence of coactivators called the LXXLL motif (SRC-1; 689–706 AA), and the ligand-binding domain of human RAR α (RAR α LBD, 156–421 AA, GenBank NM_000964). The orientation of N- and C-terminal fragments were circularly permuted in such a way that the ALuc16 reporter protein expressing the amino acids (AA) of the C-terminal fragment followed by the N-terminal fragment; this can minimize nonspecific background signal upon expression in cells. The C- and N-terminal fragments were connected via a two AA linker with glycine and serine. We generated probes using ALuc16 fragments based on seven rationally designed split sites. We previously named this design as “circularly permuted single-chain probes”.²²

Based on our previous experience, maintaining a few AA overlapping at the junction of split sites results in better complementation and improved BL intensity when compared to nonoverlapping fragments.²³ Therefore, we further created a series of BL probes, each with a pair of overlapping N- and C-terminal fragments of ALuc16 (Sara #8–Sara #13) having different overlapping lengths, ranging from 8 to 30 AA (Figure 1A). We tested all these probes in transiently transfected MDA-MB-231 breast cancer cells in the presence and absence of 10⁻⁶ M of at-RA. Upon at-RA stimulation of cells expressing the probes, the expectation would be for the at-RA to bind to RAR α LBD and induce a conformational change by repositioning the helix number 12 (H12) of the receptor and the following recruitment of coactivators.³ We designed our probes in such a way that the ligand-activated RAR α LBD binds to the adjacent LXXLL motif positioned within the single-chain probe, and which, in turn, approximates the N- and C-terminal fragments of split-ALuc16 of the fusion protein to restore the ALuc16 enzymatic activity in a RA-dependent manner.

The design of the ALuc sensors constructed for measuring RA activation used in this study is similar to what we have published previously, but the use of overlapping fragments and

the application of the sensors are different. The limitation of FRET and split reporter-based complementation systems are that the designs are not universal for all given proteins or protein partners. Every construct needs a separate optimization for the linker lengths, and the orientation for the places of the protein partners within the fusion protein. Hence, we argue that the optimal sensor designed in this study is important for studying ligand-induced activation of RAR and its biological role in various conditions.

It is difficult to completely predict and control the molecular and structural changes occurring inside the single-chain probes. We cannot exclude the probability that purified single-chain probes could have distinctive sensorial properties as those shown in the present study.

Characterization of Single-Chain BL Probes to Identify the Optimal Probe Possessing Best Signal-to-Noise Ratio in Measuring RA Activities. To identify an efficient single-chain probe, we first examined the absolute BL intensities of all single-chain probes in the presence and absence of at-RA at 10⁻⁶ M concentration (Figure 2A). We designed single-chain probes under two different categories according to molecular designs: one consisted of non-overlapping fragments of ALuc16 (Sara #1–#7), and the other carried overlapping fragments of ALuc16 with various lengths of overlap ranging from 8 to 30 AA (Sara #8–#13). As expected, the absolute levels of optical intensities of the probes with overlapping fragments were generally higher than those with nonoverlapping fragments. Notably, Sara #8 and Sara #13 showed poor optical intensities when compared to other probes. The best signal-to-background ratio (S/B) (4.0-fold) and the best absolute intensity (3.3-fold) were achieved from cells transfected with Sara #2 (nonoverlapping fragments) and Sara #12 (fragments with 24 AA overlapping), respectively. This intensity profile mirrored the general findings of our previous studies, where we have used split-FLuc probes with overlapping luciferase fragments.^{23,24}

We constructed respective control probes named Sara #2ctrl and Sara #12ctrl, where we eliminated the LXXLL motif of

Sara #2 and Sara #12, which showed minimum background signal, with negligible activation in the presence of at-RA. These results likely signify that the α -helical LXXLL motif is an essential component for ligand-activated intramolecular PPI in the single-chain probes. These findings are also in accordance with our previous study where we showed the importance of the LXXLL motifs within fluorescence resonance energy transfer (FRET) probes that carry the LBD of androgen receptor (AR).²⁵

Determination of at-RA Sensitivity in MDA-MB-231 Cells Stably Expressing RAR Probes of Overlapping and Nonoverlapping Fragments. Since the best S/B and optical intensities from our initial screening of over 13 single-chain probes were found with Sara #12 and Sara #2 of overlapping and nonoverlapping fragments respectively, we further established four different MDA-MB-231 breast cancer cell lines stably expressing Sara #2, Sara #2ctrl, Sara #12, and Sara #12ctrl probes at equal levels of expression through sorting the stable cells using the coexpressed dTomato as a normalization marker for isolating cells with equal number of delivered constructs for further RA dose–response validation. We measured the optical intensities of these cell lines in the presence and absence of different doses of at-RA ranging from 10^{-6} and 10^{-9} M. We observed a dramatic enhancement of the optical intensities in live MDA-MB-231 cells stably expressing Sara #12 compared to cells expressing Sara #2 and control probes (Figure 2B). The at-RA stimulated BL intensities were 5.2-fold stronger in MDA-MB-231 cells expressing Sara #12 than in the vehicle-stimulated cells (hereafter “vehicle” means a mock stimulator that is a PBS or Medium with the amount of organic solvent (DMF) equal to the amount used in ligand treatment). In contrast, the cells stably expressing Sara #2ctrl and Sara #12ctrl did not show any significant enhancement in BL intensities in response to at-RA. The absolute optical intensities of live MDA-MB-231 cells stably expressing Sara #2, Sara #2ctrl, or Sara #12ctrl were ~ 5 -fold less than those obtained in cells stably expressing Sara #12. We also observed these trends in lysates of MDA-MB-231 cells stably expressing Sara #2, Sara #2ctrl, Sara #12, or Sara #12ctrl (Suppl. Figure 1A), and with the MDA-MB-231 cells stably expressing Sara #12 or Sara #12ctrl cultured in 6-channel microslides (Figure 3D).

The 6-channel microslide has several advantage for imaging in cells: (i) We can image live cells with a minimal volume of medium without disturbing the cells, (ii) It is a model study that is applicable to lab-on-chips, and (iii) The size of the microslide fits into the sample stage of many microscopes, hence, imaging at the single cell level in a microscope followed by whole well imaging using an optical imaging camera is possible when using this system.

Biosensing Specificity of MDA-MB-231 Cells Stably Expressing RAR Probe Sara #12 in Response to Various Nuclear Receptor Ligands. We further determined the biosensing property of Sara #12 for its specificity and selectivity to at-RA in MDA-MB-231 cells stably expressing Sara #12 (Figure 3). We tested at-RA along with several other natural and synthetic ligands of different nuclear receptors. The ligand selectivity results showed that Sara #12 was selectively stimulated and emits BL signal when using at-RA, but not after exposure to any other natural steroid hormones, such as 17β -estradiol (E_2), cortisone, or synthetic estrogens such as hydroxytamoxifen (OHT) or diethylstilbestrol (DES) (Figure 3A). In contrast, the cells expressing Sara #12ctrl showed

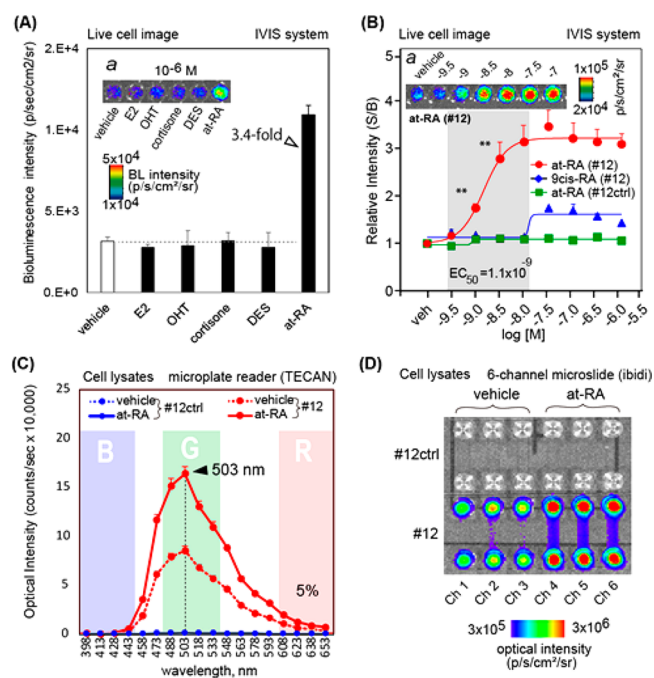


Figure 3. (A) Ligand selectivity of live MDA-MB-231 cells stably expressing Sara #12. Inset shows the optical image of cells treated with different ligands. The gray line indicates the overall basal intensity. Abbreviations: vehicle, a PBS solution containing 0.1% DMSO; E_2 , 17β -estradiol; OHT, 4-hydroxytamoxifen; DES, diethylstilbestrol; at-RA, all-trans retinoic acid. (B) Dose–response curves of BL from live MDA-MB-231 cells stably expressing Sara #12ctrl or Sara #12 in response to at-RA or 9cis-RA. Inset highlights the relative optical intensities. The p -value (student’s t test) is $** \leq 0.01$, which was compared with BL intensities of the control. (C) BL spectra of MDA-MB-231 cells stably expressing Sara #12ctrl or Sara #12. The cells were stimulated with vehicle (gray filled circles) or at-RA (black filled circles). The sequential BL intensities according to wavelengths were determined from 398 to 653 nm in 15 nm increments. The reddish shadow highlights a wavelength region longer than 600 nm. (D) Optical image of the relative BL intensities of MDA-MB-231 cells stably expressing Sara #12ctrl or Sara #12 in a 6-channel microslide (ibidi). The left 3 channels (Ch) were stimulated with vehicle, whereas the right 3 channels were incubated with at-RA for 5 h.

neither activation by at-RA nor by natural steroid hormones and synthetic estrogens. The chemical structures of the ligands were illustrated in Suppl. Figure 2. The dose–response curve with MDA-MB-231 cells stably expressing Sara #12 also demonstrated a strong elevation of BL signal at around $10^{-9.5}$ M of at-RA, reaching a plateau at $\sim 10^{-8}$ M (Figure 3B). The effective concentration at 50% (EC_{50}) activation for at-RA was 1.1×10^{-9} M according to data analysis performed using Prism 7.0 (GraphPad). Interestingly, the linear range observed in this study was almost equivalent to that of a previous BRET probe using the same RAR α LBD, reported by Shimozono et al.¹³ The dose–response profile showed that Sara #12 would be sufficiently sensitive to determine the endogenous levels of at-RA in living mice, considering that the levels in serum and tissues are reported to be $\sim 1.9 \times 10^{-9}$ M and 7.0 – 9.6×10^{-9} M, respectively.²⁶ This high sensitivity of Sara #12 could therefore allow us to determine at-RA levels in cells obtained by biopsies of living subjects.

We also determined the overall BL spectra of MDA-MB-231 cells stably expressing Sara #12 or Sara #12ctrl using a

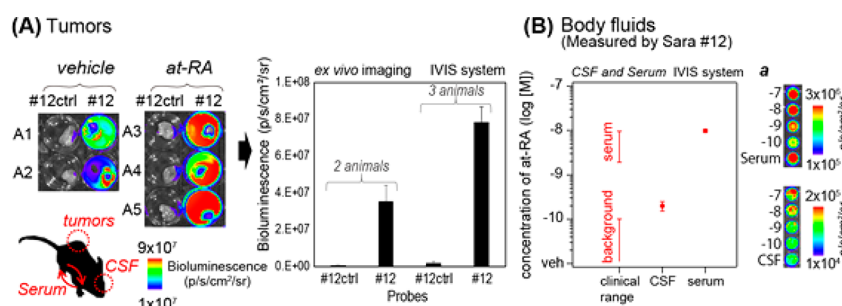


Figure 4. (A) Ex vivo BL image of tumor tissues collected from five mice 3 weeks after implantation of MDA-MB-231 cells stably expressing Sara #12ctrl or Sara #12. The corresponding BL intensities were determined using an IVIS Lumina II imaging system (PerkinElmer, USA) by the addition of nCTZ. The arrow points to the quantitative analysis of the BLI from the ex vivo images of tumor tissues. (B) Determination of endogenous levels of RAs in CSF and serum of mouse. Inset a shows the typical BL intensities in response to the ligand stimulators. Abbreviations: veh, background (vehicle stimulation); CSF, cerebrospinal fluid.

microplate reader equipped with automatically revolving optical filters (Figure 3C). The maximal optical intensities (λ_{\max}) of Sara #12 and Sara #12ctrl were commonly found at 503 nm, and approximately 5% of the total optical intensity was observed beyond 600 nm. The green BL peak of Sara #12 embedding the fragments of ALuc16 (~500 nm) was exactly equivalent to that of intact full-length ALuc16. We also found that at-RA selectively elevates the BL intensities of MDA-MB-231 cells expressing Sara #12 throughout all the wavelengths (Figure 3C), whereas it did not show any enhanced intensities in cells expressing Sara #12ctrl at the similar wavelength range (Supporting Figure 3A). The AA sequence of Sara #12 are illustrated in Supporting Figure 5.

The overall comparison of the results between Sara #12 and #12ctrl may be explained as follows: (i) The LXXLL motif is an essential ingredient for intramolecular PPI of Sara #12. (ii) The ~5-fold stronger background intensities of Sara #12 than those of Sara #12ctrl may reflect a basal, nonspecific PPI between the LXXLL motif and the RAR α LBD positioned inside Sara #12 in the absence of at-RA. (iii) The basal PPI may happen through nongenomic pathways activated by metabolites in the culture medium or the conformational change induced by the interaction of other cellular proteins, as discussed before;^{27,28} and (iv) In accordance with the λ_{\max} of Sara #12 and Sara #12ctrl, intramolecular complementation indeed occurs between the split N- and C-terminal fragments of ALuc16 inside the probes, considering the λ_{\max} of ALuc16 is known to be at ~500 nm.^{29,30}

Ex Vivo BL Imaging of Tumor Tissues Extracted from Mice Bearing MDA-MB-231 Tumor Xenografts Stably Expressing Sara #12 or Sara #12ctrl. The in vivo imaging of ligand-activated signal would be a useful technique for measuring ligand biodistribution in different organs. Since the absolute signal achieved from split reporter-based complementation systems are a very small percentage of full-length luciferase,^{31,32} our attempt at in vivo imaging for endogenous RAR-activated sensor signal in living mice bearing tumor xenografts of MD-MB-231 cells showed poor light output. This, in part, was owing to the ALuc16 emission in the green spectrum with a peak wavelength of ~500 nm, which is normally absorbed by biological tissues in vivo.³³ Hence after tumor sizes reached ~4–5 mm in diameter, we collected tissues of tumors stably expressing Sara #12 and its respective control probe Sara #12ctrl from the same animal, and we performed ex vivo optical BL imaging. We obtained ex vivo images from samples extracted from five mice-bearing tumors

stably expressing either Sara #12 or Sara #12ctrl (Figure 4). We weighed left and right tumors and found the tumor sizes were equivalent in each mouse as follows: [0.62 and 0.62 g] for Mouse 1, [0.35 and 0.32 g] for Mouse 2, [0.65 and 0.71 g] for Mouse 3, [0.53 and 0.57 g] for Mouse 4, and [0.51 and 0.57 g] for Mouse 5.

Tumor tissues expressing Sara #12ctrl clearly showed the weakest BL intensities, which were almost at background levels regardless of stimulation of at-RA or vehicle. In contrast, tumor tissues expressing Sara #12 showed a significant variation according to the presence or absence of at-RA. The at-RA-treated group showed an average 2.2-fold enhanced BL intensities (Figure 4A).

We found that the S/B ratio in the ex vivo imaging was relatively less than the corresponding cell-based imaging results discussed above, which was nearly 5.2-fold in response to at-RA (Figure 2B). This feature can be explained with reference to the role of endogenous at-RA. Its levels are high enough to half saturate Sara #12 and #12ctrl in mouse tissues,²⁶ when considering the dose–response curve of Sara #12. Thus, these relatively low S/B ratios may be attributable to a background drift by endogenous at-RA.

We recorded the BL decay rates from tumor tissues stably expressing Sara #12 or Sara #12ctrl (Suppl. Figure 4). We found that BL reached the half point of maximal intensity after 13 min and was stable for up to 30 min after substrate injection.

The split-reporter complementation system may be dimmer than the other full-length reporter system. The intensity mainly depends on the efficiency of PPIs or protein foldings, which facilitate the split fragments aligning in a better orientation for the reconstitution of the enzymatic pocket of the reporter. The corresponding in vivo imaging also depends on the emission wavelength of these optical reporters. The use of split fragments of a luciferase with the emission wavelength of above 600 nm provides brighter images than the other split-luciferases emitting blue or green light, if all other conditions are equivalent.

The above results show that Sara #12 can quantitatively image at-RA-driven RAR activities in human MDA-MB-231 cells, including those obtained from tumor tissues. This result opens a new means possibly to investigate cancer metastases, considering the diverse roles of at-RA in cancer metastasis. At-RA efficiently inhibits the growth, metastasis, and differentiation of xenograft tumors^{34,35} and various breast cancers.³⁶ Future studies will therefore require construction of a similar

system that uses a red-shifted optical reporter with less light attenuation in biological tissues *in vivo* to further explore the use of this important sensor in oncogenesis and anticancer effect of at-RA.

Determination of at-RA Levels in Serum and Cerebrospinal Fluid. We further tested the sensitivity of the RAR probe Sara #12 in measuring RA levels in mouse serum and cerebrospinal fluid (CSF) (Figure 4B). We used cells stably expressing Sara #12 and found that the standard solutions of at-RA produced a slope of BL intensities in a concentration-dependent manner. Based on the calibration curves, we observed the endogenous levels in serum and CSF samples to be $9.8 (\pm 0.7) \times 10^{-9}$ M and $2.0 (\pm 0.5) \times 10^{-10}$ M, respectively. We compared the endogenous at-RA levels with the known clinical range in mouse body fluids in Figure 4B. Considering that the clinical range of at-RA in serum and tissues is approximately $1.9\text{--}9.6 \times 10^{-9}$ M,²⁶ our observed values were found to be at the upper end of the clinical range. This relatively high concentration may be partly contributed by nongenomic RAR activators^{27,28} and other RA isomers besides at-RA, such as 9-cis-RA and 13-cis-RA in serum. On the other hand, CSF induced a basal BL intensity level (2.0×10^{-10} M). This suggests that CSF does not contain a considerable level of at-RAs. This result corroborates the findings of a previous study,³⁷ where no at-RA in CSF was detected by liquid chromatography or mass spectrometry.

CONCLUSION

RA is a key metabolite in the development and differentiation in vertebrates. Here, we demonstrate a highly sensitive BL imaging approach with a genetically encoded, ligand-activatable single-chain probe to quantitatively measure the biological impacts of at-RA in live mammalian cells. We tested 13 molecular designs of the single-chain probes and identified the one that performed best in quantitative imaging of at-RA activities in live cells, xenografts, and in different body fluids (e.g., mouse serum and CSF). The described method expands the arsenal of bioassays to measure RAs from biological sources. In contrast to FRET-based imaging technologies where complex analytical tools are needed to distinguish activated FRET signal, the present ligand-activatable single-chain probe provides a straightforward assay where BL signals can be directly correlated with the level of at-RA activities. This BL-based assay has advantages over other methods, for instance: (i) no interference of background light, (ii) no requirement of excitation light source, and (iii) no requirement of a sophisticated light filtration system. Thus, we present a new imaging-based tool to investigate various RA-activated molecular events, potentially applicable to the study of cell growth and differentiation, nervous system development, pattern formation, tumorigenesis, and in many other diseases.

EXPERIMENTAL PROCEDURES

Engineering Vectors Encoding cDNA Constructs of Single-Chain BL Probes for RA Activities. We engineered single-chain probes by a tandem linkage of four different protein components, that is, human RAR α LBD (156–421 AA, GenBank NM_000964), the N-terminal domain of artificial luciferase 16 (ALuc16, GenBank MF817967) (19–x-1 AA; \textcircled{N} -ALuc16), the C-terminal domain of ALuc16 (x–211 AA; \textcircled{C} -ALuc16), and the α -helical LXXLL motif (689–706 AA) from SRC-1 coactivator protein (Figure 1).

We constructed a series of cDNA constructs encoding Sara #1–#13 according to the experimental workflow as shown in Figure 1. Each cDNA block was made by PCR amplification to introduce required restriction enzyme sites: (i) *HindIII/BamHI* to the cDNA encoding the LXXLL motif, (ii) *BamHI/AgeI* to the cDNA encoding the \textcircled{C} -ALuc16, (iii) *AgeI/KpnI* to the cDNA encoding the \textcircled{N} -ALuc16, and (iv) *KpnI/XhoI* to the cDNA encoding RAR α LBD. The amplified cDNA blocks were digested with the respective restriction enzymes, purified, ligated, and subcloned into the corresponding restriction enzyme-digested pcDNA3.1(+) vector backbone with a cytomegalovirus (CMV) enhancer-promoter (Invitrogen) or pHAGE lentiviral backbone with a CMV enhancer-promoter for the expression of the sensors used for the study. The corresponding vectors were named as pSara #1 to pSara #13. For simplification, the expressed single-chain probes were named as Sara #1 to Sara #13.

As a reference, we made control vectors for Sara #2 and #12, where the cDNA encoding the LXXLL motif was removed from the cDNA construct as shown in Figure 1B. We named the plasmids pSara #2-ctrl and pSara #12-ctrl, respectively; and named the control probes after expression, Sara #2ctrl and Sara #12ctrl, respectively. We tested the fidelity of the cDNA constructs using a genetic sequence analyzer by order (Eurofin genomics).

Determination of RA Activities Using MDA-MB-231 Cells Transiently Transfected with pSara #1–#13. We plated MDA-MB-231 cells in a 96-well microplate and incubated to reach 80% confluence in 24 h by incubating at 37 °C incubator with 5% CO₂. We then transiently transfected the cells with pSara #1–#13 using Lipofectamine 2000 transfection reagent (Invitrogen, Carlsbad, CA) by following manufacturer's instruction, and incubated further for 24 h. The culture media of the cells were replaced with media dissolving a vehicle or 10⁻⁶ M at-RA, and further incubated for 5 h. We prepared the cell lysates according to the technical instructions of the *Renilla* luciferase assay kit (Promega, Madison, WI), and determined the ligand activated complementation activities of ALuc16 fragments of Sara #1–#13 in the lysates using an IVIS Lumina II imaging system (PerkinElmer, USA) immediately after simultaneous injection of the assay solution dissolving native coelenterazine (nCTZ) using a multichannel micropipette (Figure 2A).

Determination of RA Activities Using MDA-MB-231 Cells Stably Expressing Sara #2 and #12. As Sara #2 and #12 showed relatively high optical intensities and/or S/Bs compared to the other probes, we subcloned the cDNA constructs encoding Sara #2, #2ctrl, #12, #12ctrl into the backbones of pcDNA 3.1(+) puromycin vectors. We transfected each plasmid into MDA-MB-231 cells and incubated in a puromycin-added (100 ng/mL) Dulbecco's Modified Eagle Medium (DMEM) supplemented with 5% FBS and 1% P/S. We selected the positive clones by long-term culturing and serial passage of the MDA-MB-231 cells.

We seeded the MDA-MB-231 cells stably expressing Sara #2, Sara #2ctrl, Sara #12, or Sara #12ctrl in 96-well optical bottom black wall microplates and cultured for 1 day. We then stimulated the cells in the microplates for 5 h using 10⁻⁹ M and 10⁻⁶ M of at-RA, or the vehicle. Half of the wells culturing live cells remained untreated and we lysed the other half using the same method described in Figure 2A. We separately determined the corresponding BL intensities from the live cells or the lysates using the IVIS Lumina II imaging system

(PerkinElmer, USA) after injection of a PBS buffer dissolving nCTZ using a multichannel micropipette. The BL intensities from live cells and lysates are shown in [Figure 2B](#) and [Supporting Figure 1A](#), respectively.

We further investigated the ligand selectivity of the MDA-MB-231 cells stably expressing #12 ([Figure 3A](#)). We plated the cells in 96-well optical bottom microplates, and stimulated with 10^{-6} M of E_2 , OHT, cortisone, DES, at-RA, or vehicle (0.1% DMSO) for 5 h. The corresponding BL intensities from the ligand-stimulated MDA-MB-231 cells were determined using the IVIS Lumina II imaging system (PerkinElmer, USA) after simultaneous injection of a PBS buffer dissolving nCTZ using a multichannel micropipette.

Dose–Response Curves of Sara #12 and Sara #12ctrl. After evaluating ligand specificity, we further determined the corresponding dose response curves in the concentration range from $10^{-9.5}$ to 10^{-6} M of at-RA. We plated the MDA-MB-231 cells stably expressing Sara #12 or Sara #12ctrl and incubated in 96-well clear bottom black wall microplates. The cells were then stimulated with varying concentrations of the at-RA for 5 h. After decanting the cell media, the cells were simultaneously added with a PBS buffer dissolving nCTZ (10 $\mu\text{g}/\text{mL}$). We determined the corresponding BL intensities using the IVIS Lumina II imaging system (PerkinElmer, USA), and analyzed with Living Image ver 4.5. We analyzed the sigmoidal curves using Prism version 7 for calculating the EC_{50} values.

BL Imaging of Living MDA-MB-231 Cells Expressing Sara #12 or Sara #12ctrl in Microslide. We plated MDA-MB-231 cells stably expressing Sara #12ctrl or Sara #12 in a 6-channel microslide and incubated overnight. We stimulated the cells for 5 h using vehicle (0.1% methanol) or 10^{-6} M of at-RA. The culture medium in each channel of the microslide was replaced with an aliquot (40 μL) of a lysis buffer (Promega, Madison, WI) and further incubated for 20 min. We simultaneously mixed the lysates in the channels with an assay buffer (Promega, Madison, WI) dissolving nCTZ using a multichannel micropipette. The optical images were immediately determined using the IVIS Lumina II imaging system (PerkinElmer, USA).

Determination of BL Spectra of Sara #12ctrl and Sara #12. We also determined the BL spectra of Sara #12ctrl and Sara #12 using vehicle- or at-RA-stimulated MDA-MB-231 cells ([Figure 3C](#)). We plated MDA-MB-231 cells stably expressing Sara #12ctrl or Sara #12 in 96-well optical-bottom microplates and incubated overnight in a cell incubator. We stimulated the cells using 10^{-6} M of at-RA or vehicle (0.1% methanol). The cells in the microplates were lysed using a lysis buffer (Promega, Madison, WI), and the lysates were simultaneously mixed with an assay buffer (Promega, Madison, WI) containing 10 $\mu\text{g}/\text{mL}$ of nCTZ. We immediately determined the sequential optical intensities according to wavelengths using a microplate reader (Spark 10M, TECAN) by automatically revolving the optical filters ranging from 398 to 653 nm in 15 nm increments (each filter has a 15 nm band window).

Ex Vivo Imaging of Mouse Tumor Samples. We purchased 8-week old female BALB/c mice from Charles River Wilmington, MA, USA). Five animals were housed in each cage under a light-dark (12 h/12 h) cycle with ad libitum access to water and food. We performed experimental manipulations under inhalation anesthesia induced by a 4% (and maintained by 2.3%) mixture of isoflurane in oxygen administered through facial masks.

We suspended the MDA-MB-231 cells stably expressing Sara #12 or Sara #12ctrl, in 50 μL of PBS and mixed with 50 μL Matrigel, and implanted them subcutaneously in the left (Sara #12ctrl) and right (Sara #12) sides of the lower flank. We waited 3 weeks until the tumor sites stabilized and there was sufficient tumor growth for BL imaging.

We ex vivo imaged the mouse tumor tissues. The left and right tumor sizes of each mouse were almost equivalent. We surgically extracted the tumor tissues from the five mice that were sacrificed under inhalation anesthesia. The tumor tissues were stored in a 12-well microplate under immersion of 3 mL of PBS buffer per well, and stored in the cold room for 2 days to reduce the endogenous cortisol levels.

Before ex vivo imaging, we prepared two substrate cocktails; Cocktail A was a PBS buffer dissolving nCTZ and vehicle (0.1% methanol); Cocktail B was a PBS buffer carrying nCTZ and 10^{-6} M of at-RA. We then determined the ex vivo BL intensities using the IVIS Lumina II imaging system (Perkin Elmer, USA) immediately after replacing the immersing buffer with Cocktail A or Cocktail B. We measured the BL intensity change every 5 min to monitor the BL decay. We analyzed the corresponding images using Living Image, version 4.5 (Caliper) ([Figure 4](#)).

Determination of at-RA Levels in Mouse Serum and Cerebrospinal Fluid. We studied the endogenous at-RA levels in serum and cerebrospinal fluid (CSF) using MDA-MB-231 cells stably expressing Sara #12. We plated the cells in 96-well black frame clear bottom microplates and cultured for 1 day. The cells were then starved for 5 h through replacing the culture medium with a DMEM without fetal bovine serum. We stimulated the cells for 4 h with varying concentrations of at-RAs or 1:1 mixture of mouse serum or CSF with DMEM without FBS. The cells were then washed once with a PBS buffer and lysed for 20 min with a Promega lysis buffer. The cell lysates were then illuminated by simultaneously injecting a 100 μL of the substrate solution (nCTZ) into the wells using an 8-channel micropipette. We imaged the corresponding BL intensities using the IVIS Lumina II imaging system (PerkinElmer, USA). We analyzed the BL images using Living Image, version 4.5.5.

■ ASSOCIATED CONTENT

📄 Supporting Information

The Supporting Information is available free of charge on the ACS Publications website at DOI: [10.1021/acscombsci.9b00035](https://doi.org/10.1021/acscombsci.9b00035).

Relative optical intensities of MDA-MB-231 cells stably expressing Sara #12ctrl, or #12 in microplates and 6-channel microslides; chemical structures of ligands we used; BL spectra of MDA-MB-231 cells stably expressing Sara #12ctrl or #12; time course of ex vivo BL intensities from tumor tissues stably expressing Sara #12ctrl or Sara #12; and schematic diagram of the amino acid sequence of Sara #12 ([PDF](#))

■ AUTHOR INFORMATION

Corresponding Authors

*E-mail: kimu-sb@aist.go.jp.

*E-mail: paulmur8@stanford.edu.

ORCID

Sung Bae Kim: [0000-0002-7033-9056](https://orcid.org/0000-0002-7033-9056)

Daniel Citterio: [0000-0001-7420-045X](https://orcid.org/0000-0001-7420-045X)

Tarik F Massoud: 0000-0002-9694-1408

Ramasamy Paulmurugan: 0000-0001-7155-4738

Author Contributions

S.B.K, D.C., K.S., T.M., and R.P. conceived and designed the experiments; S.B.K, R.F., R.N., R.B., and R.P. performed the experiments; S.B.K, D.C., K.S., T.M., and R.P. cowrote the manuscript and Supporting Information; all authors reviewed the manuscript and Supporting Information.

Notes

The authors declare no competing financial interest.

ACKNOWLEDGMENTS

This work was partly supported by JSPS KAKENHI Grants: 26288088, 15KK0029, 16K14051, 17H01215, and 24225001.

REFERENCES

- (1) Lamour, F. P.; Lardelli, P.; Apfel, C. M. Analysis of the ligand-binding domain of human retinoic acid receptor alpha by site-directed mutagenesis. *Mol. Cell. Biol.* **1996**, *16* (10), 5386–5392.
- (2) Niederreither, K.; Subbarayan, V.; Dollé, P.; Chambon, P. Embryonic retinoic acid synthesis is essential for early mouse post-implantation development. *Nat. Genet.* **1999**, *21*, 444–448.
- (3) Le Maire, A.; Teyssier, C.; Erb, C.; Grimaldi, M.; Alvarez, S.; De Lera, A. R.; Balaguer, P.; Gronemeyer, H.; Royer, C. A.; Germain, P.; Bourguet, W. A unique secondary-structure switch controls constitutive gene repression by retinoic acid receptor. *Nat. Struct. Mol. Biol.* **2010**, *17* (7), 801–807.
- (4) Kurtz, P. J.; Emmerling, D. C.; Donofrio, D. J. Subchronic toxicity of all-trans-retinoic acid and retinylidene dimedone in Sprague-Dawley rats. *Toxicology* **1984**, *30* (2), 115–124.
- (5) Hixson, E. J.; Burdeshaw, J. A.; Denine, E. P.; Harrison, S. D. J. Comparative subchronic toxicity of all-trans- and 13-cis-retinoic acid in Sprague-Dawley rats. *Toxicol. Appl. Pharmacol.* **1979**, *47* (2), 359–365.
- (6) Allen, L. H.; Haskell, M. Estimating the Potential for Vitamin A Toxicity in Women and Young Children. *J. Nutr.* **2002**, *132* (9), 2907S–2919S.
- (7) Nau, H. Teratogenicity of isotretinoin revisited: Species variation and the role of all-trans-retinoic acid. *J. Am. Acad. Dermatol.* **2001**, *45* (5), S183–S187.
- (8) Leung, M. C. K.; Phuong, J.; Baker, N. C.; Sipes, N. S.; Klinefelter, G. R.; Martin, M. T.; McLaurin, K. W.; Setzer, R. W.; Darney, S. P.; Judson, R. S.; Knudsen, T. B. Systems Toxicology of Male Reproductive Development: Profiling 774 Chemicals for Molecular Targets and Adverse Outcomes. *Environ. Health Perspect.* **2016**, *124* (7), 1050–1061.
- (9) Altucci, L.; Gronemeyer, H. The promise of retinoids to fight against cancer. *Nat. Rev. Cancer* **2001**, *1* (3), 181–193.
- (10) Njar, V. C. O.; Gediya, L.; Purushottamachar, P.; Chopra, P.; Vasatis, T. S.; Khandelwal, A.; Mehta, J.; Huynh, C.; Belosay, A.; Patel, J. Retinoic acid metabolism blocking agents (RAMBAs) for treatment of cancer and dermatological diseases. *Bioorg. Med. Chem.* **2006**, *14* (13), 4323–4340.
- (11) Zachara, N. E.; Hart, G. W. The emerging significance of O-GlcNAc in cellular regulation. *Chem. Rev.* **2002**, *102* (2), 431–438.
- (12) Balkan, W.; Colbert, M.; Bock, C.; Linney, E. Transgenic Indicator Mice for Studying Activated Retinoic Acid Receptors during Development. *Proc. Natl. Acad. Sci. U. S. A.* **1992**, *89* (8), 3347–3351.
- (13) Shimozono, S.; Iimura, T.; Kitaguchi, T.; Higashijima, S.; Miyawaki, A. Visualization of an endogenous retinoic acid gradient across embryonic development. *Nature* **2013**, *496* (7445), 363–366.
- (14) Schüle, R.; Rangarajan, P.; Yang, N.; Kliever, S.; Ransone, L. J.; Bolado, J.; Verma, I. M.; Evans, R. M. Retinoic acid is a negative regulator of AP-1-responsive genes. *Proc. Natl. Acad. Sci. U. S. A.* **1991**, *88* (14), 6092–6096.
- (15) Parsons, S. J. W.; Rhodes, S. A.; Connor, H. E.; Rees, S.; Brown, J.; Giles, H. Use of a dual firefly and Renilla luciferase reporter gene

assay to simultaneously determine drug selectivity at human corticotrophin releasing hormone 1 and 2 receptors. *Anal. Biochem.* **2000**, *281* (2), 187–192.

- (16) Fan, F.; Wood, K. V. Bioluminescent assays for high-throughput screening. *Assay Drug Dev. Technol.* **2007**, *5* (1), 127–136.

- (17) Kim, S. B.; Otani, Y.; Umezawa, Y.; Tao, H. Bioluminescent indicator for determining protein-protein interactions using intramolecular complementation of split click beetle luciferase. *Anal. Chem.* **2007**, *79* (13), 4820–4826.

- (18) Kim, S. B.; Awais, M.; Sato, M.; Umezawa, Y.; Tao, H. Integrated molecule-format bioluminescent probe for visualizing androgenicity of ligands based on the intramolecular association of androgen receptor with its recognition peptide. *Anal. Chem.* **2007**, *79* (5), 1874–1880.

- (19) Kim, S. B.; Takenaka, Y.; Torimura, M. A Bioluminescent Probe for Salivary Cortisol. *Bioconjugate Chem.* **2011**, *22* (9), 1835–1841.

- (20) Kim, S. B.; Umezawa, Y.; Kanno, K. A.; Tao, H. An integrated-molecule-format multicolor probe for monitoring multiple activities of a bioactive small molecule. *ACS Chem. Biol.* **2008**, *3* (6), 359–372.

- (21) Kim, S. B.; Torimura, M.; Tao, H. Creation of artificial luciferases for bioassays. *Bioconjugate Chem.* **2013**, *24* (12), 2067–2075.

- (22) Kim, S. B.; Sato, M.; Tao, H. Circularly Permutated Bioluminescent Probes for Illuminating Ligand-Activated Protein Dynamics. *Bioconjugate Chem.* **2008**, *19* (12), 2480–2486.

- (23) Paulmurugan, R.; Gambhir, S. S. Combinatorial library screening for developing an improved split-firefly luciferase fragment-assisted complementation system for studying protein-protein interactions. *Anal. Chem.* **2007**, *79* (6), 2346–2353.

- (24) Paulmurugan, R.; Gambhir, S. S. Firefly luciferase enzyme fragment complementation for imaging in cells and living animals. *Anal. Chem.* **2005**, *77* (5), 1295–1302.

- (25) Van Royen, M. E.; Cunha, S. M.; Brink, M. C.; Mattern, K. A.; Nigg, A. L.; Dubbink, H. J.; Verschure, P. J.; Trapman, J.; Houtsmuller, A. B. Compartmentalization of androgen receptor protein-protein interactions in living cells. *J. Cell Biol.* **2007**, *177* (1), 63–72.

- (26) Kane, M. A.; Chen, N.; Sparks, S.; Napoli, J. L. Quantification of endogenous retinoic acid in limited biological samples by LC/MS/MS. *Biochem. J.* **2005**, *388*, 363–369.

- (27) Masia, S.; Alvarez, S.; De Lera, A. R.; Baretino, D. Rapid, nongenomic actions of retinoic acid on phosphatidylinositol-3-kinase signaling pathway mediated by the retinoic acid receptor. *Mol. Endocrinol.* **2007**, *21* (10), 2391–2402.

- (28) Farrar, N. R.; Dmetrichuk, J. M.; Carlone, R. L.; Spencer, G. E. A Novel, Nongenomic Mechanism Underlies Retinoic Acid-Induced Growth Cone Turning. *J. Neurosci.* **2009**, *29* (45), 14136–14142.

- (29) Kim, S. B.; Miller, S.; Suzuki, N.; Senda, T.; Nishihara, R.; Suzuki, K. Cation-driven Optical Properties of Artificial Luciferases. *Anal. Sci.* **2015**, *31* (10), 955–960.

- (30) Kim, S. B.; Nishihara, R.; Citterio, D.; Suzuki, K. Fabrication of a New Lineage of Artificial Luciferases from Natural Luciferase Pools. *ACS Comb. Sci.* **2017**, *19* (9), 594–599.

- (31) Paulmurugan, R.; Umezawa, Y.; Gambhir, S. S. Noninvasive imaging of protein-protein interactions in living subjects by using reporter protein complementation and reconstitution strategies. *Proc. Natl. Acad. Sci. U. S. A.* **2002**, *99* (24), 15608–15613.

- (32) Paulmurugan, R.; Gambhir, S. S. Monitoring protein-protein interactions using split synthetic renilla luciferase protein-fragment-assisted complementation. *Anal. Chem.* **2003**, *75* (7), 1584–1589.

- (33) Weissleder, R.; Ntziachristos, V. Shedding light onto live molecular targets. *Nat. Med.* **2003**, *9* (1), 123–128.

- (34) Chen, Y. Q.; Wu, Q.; Chen, Z. M.; Chen, F.; Su, W. J. Effect of all-trans retinoic acid on growth of xenograft tumor and its metastasis in nude mice. *Chinese Med. J.* **2000**, *113* (4), 345–349.

- (35) Shalinsky, D. R.; Bischoff, E. D.; Gregory, M. L.; Gottardis, M. M.; Hayes, J. S.; Lamph, W. W.; Heyman, R. A.; Shirley, M. A.;

Cooke, T. A.; Davies, P. J. A. Retinoid-Induced Suppression of Squamous-Cell Differentiation in Human Oral Squamous-Cell Carcinoma Xenografts (Line-1483) in Athymic Nude-Mice. *Cancer Res.* **1995**, *55* (14), 3183–3191.

(36) Patel, J. B.; Mehta, J.; Belosay, A.; Sabnis, G.; Khandelwal, A.; Brodie, A. M. H.; Soprano, D. R.; Njar, V. C. O. Novel retinoic acid metabolism blocking agents have potent inhibitory activities on human breast cancer cells and tumour growth. *Br. J. Cancer* **2007**, *96* (8), 1204–1215.

(37) Muindi, J. R. F.; Frankel, S. R.; Huselton, C.; Degrazia, F.; Garland, W. A.; Young, C. W.; Warrell, R. P. Clinical-Pharmacology of Oral All-Trans Retinoic Acid in Patients with Acute Promyelocytic Leukemia. *Cancer Res.* **1992**, *52* (8), 2138–2142.